Bias-free syngas production by integrating a molecular cobalt catalyst with perovskite-$BiVO_4$ tandems

Virgil Andrei,[1] Bertrand Reuillard,[1] and Erwin Reisner[1]*

The photoelectrochemical (PEC) production of syngas from water and CO_2 represents an attractive technology towards a circular carbon economy. However, the overpotential (i.e. energy loss), low selectivity and cost of commonly employed catalysts make this sustainable alternative challenging. Here, we demonstrate highly tunable PEC syngas production by integrating an earth abundant, cobalt porphyrin catalyst immobilized on carbon nanotubes with triple-cation mixed halide perovskite and $BiVO_4$ photoabsorbers. Empirical data analysis is used to clarify the optimal electrode selectivity at low catalyst loadings. The perovskite photocathodes maintain selective aqueous CO_2 reduction for one day at light intensities as low as 0.1 Sun. Perovskite-$BiVO_4$ PEC tandems sustain an unprecedented bias-free syngas production for three days with solar-to-H_2 and solar-to-CO conversion efficiencies of 0.06% and 0.02%, respectively, operating as standalone artificial leaves in neutral pH solution. These systems provide potential pathways for maximizing daylight utilisation, by sustaining CO_2 conversion even under low solar irradiance.

Syngas, a mixture of CO and H_2, is a crucial intermediate in the industrial production of methanol, higher alcohols, long-chain hydrocarbons, lubricants, waxes and fuels via the Fischer-Tropsch process.[1–3] Applications extend to pharmaceuticals, bulk chemical synthesis and fertilisers. The conventional reforming of methane to syngas relies on fossil fuels to operate at high temperatures and pressures[3] and biomass gasification can introduce contaminants.[4] The solar-driven production of syngas from aqueous CO_2 is an ambient conditions and clean alternative process.[5] Although silicon,[6] dye,[7] metal oxide,[8–10] or perovskite[11,12] photoabsorbers provide enough driving force in tandem devices for bias-free water splitting, very few examples of bias-free PEC CO_2 reduction are known.[13–16] Due to the large overpotentials which need to be overcome for simultaneous CO_2 reduction and water oxidation,[17] most of those systems employ up to six photovoltaic (PV) solar cells connected in series,[13,18,19] or complex noble metal based nanostructures.[14,16,20] Accordingly, a vast library of molecular catalysts employing earth abundant-metals for CO_2 reduction remains underexplored.[21–24] Such catalysts are known to achieve improved selectivities towards CO production at lower overpotentials, with Co porphyrin and phthalocyanin recently demonstrating selective aqueous CO_2 reduction to CO when immobilized onto carbon nanotube (CNT) based electrodes.[25–27]

Here, we tap into that library of molecular catalysts by using the commercially available cobalt(II) meso-tetrakis(4-methoxyphenyl)porphyrin (abbreviated CoMTPP), which can be readily immobilized via π-π stacking interactions[26] onto CNT sheets, also known as buckypaper (Fig. 1, right side). The composite is employed in electrodes, state-of-the-art perovskite-based photocathodes and perovskite-$BiVO_4$ PEC tandem devices, which couple tunable syngas to O_2 production in an aqueous solution (see device architecture in Fig. 1, left side).

CoMTPP@CNT electrodes

Buckypaper (2.8 mg cm^{-2}, $\approx$100 μm thickness) was incubated in a CoMTPP solution of different concentrations in N,N-dimethylformamide (DMF), followed by rinsing steps in DMF and Milli-Q water (Methods and Supplementary Fig. 1). Cyclic voltametry (CV) scans of the free-standing CoMTPP@CNT electrodes (Fig. 2a) show similar current responses in the presence of N_2 and CO_2 atmosphere against the reversible hydrogen electrode (RHE), in an aqueous 0.5 M $KHCO_3$ solution. A slight decrease in the cathodic current is observed under CO_2 at a given potential against RHE, yet not against the Ag/AgCl reference, or under stirring (Supplementary Fig. 2). This effect can be partly explained by the capacitive charging of the buckypaper, which may alter the effective applied potential at the CNT-catalyst interface. Controlled potential electrolysis (CPE) at different applied potentials supports the observed onset potential between -0.5 and -0.4 V vs. RHE for CO_2 reduction (Supplementary Fig. 3 and Table 1).

The activity of the immobilized catalyst for both CO_2 and proton reduction is confirmed by measuring 4 h CPE (see example in Supplementary Fig. 4) for buckypaper electrodes incubated in CoMTPP solutions of different concentrations (c_{CoMTPP}, Fig. 2b). For electrode optimization, CPE is conducted at -0.6 V vs. RHE, which provides the highest selectivity towards CO_2 reduction. The Co loading before and after CPE, turnover number (TON) and turnover frequency (TOF) are calculated based on inductively coupled plasma optical emission spectroscopy (ICP-OES) data (Methods, Supplementary Figs. 5, 6 and Table 2). Approximately 170 μmol cm^{-2} H_2 are produced using concentrations above 1 mM where the catalyst solution becomes saturated, whereas the CO already plateaus to $\approx$70 μmol cm^{-2} at 0.25 mM. The amounts of gases produced follow sigmoidal trends against the CoMTPP concentration, which can be analytically fitted using an empirical logistic model (details given in Supplementary Table 3). The fits support the low intrinsic activity of buckypaper towards H_2 evolution (3.03 ± 0.14 μmol cm^{-2}), whereas upper boundaries in the product formation of 199.0 ± 5.8 H_2 and 68.0 ± 3.6 μmol cm^{-2} CO are predicted at high catalyst loading. By dividing the two functions, a CO:H_2 selectivity curve is obtained (green trace in Fig. 2b), which accurately describes the experimental data, validating the sigmoid model.

The optimum selectivity towards CO production is obtained by incubating the buckypaper in a 0.05 mM CoMTPP solution (9.12$\pm$0.65 nmol cm^{-2} loading), which results in a maximum CO:H_2 ratio of 3.08$\pm$0.70 (26.3$\pm$5.4 μmol cm^{-2} CO, 8.6$\pm$0.6 μmol cm^{-2} H_2, corresponding to large TON values of 2878$\pm$627 for CO and 939$\pm$94 for H_2). These conditions are supported by the numerical fit, which indicates a maximum in selectivity at 0.047 mM CoMTPP. A higher CO selectivity is achieved when incubating the CNT sheets in less concentrated CoMTPP solutions, which seems to indicate CO_2 transport limitations at a higher catalyst loading.[25] CPE under stirring yields more CO (57.1$\pm$9.5 μmol cm^{-2}, 6259$\pm$1135 TON), but a similar amount of H_2 (7.9$\pm$1.3 μmol cm^{-2}, 866$\pm$160 TON) for the optimized samples, resulting in a 7.24$\pm$0.37 selectivity which further supports the bulk external CO_2 transport limitations (note that experiments are typically performed without stirring to simulate real device operation). Further fine-tuning of the selectivity was

[1] Christian Doppler Laboratory for Sustainable SynGas Chemistry, Department of Chemistry, University of Cambridge, Lensfield Road, Cambridge CB2 1EW, United Kingdom. *E-mail: reisner@ch.cam.ac.uk; Web: http://www-reisner.ch.cam.ac.uk

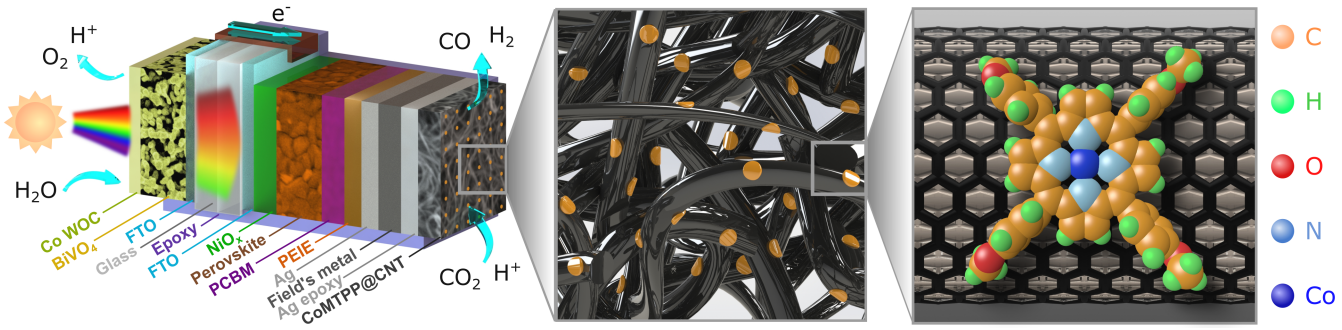

Fig. 1 | Architecture of the standalone perovskite-$BiVO_4$ PEC tandem device for bias-free syngas production. Oxygen evolution occurs at the front $BiVO_4$ photoanode with a Co water oxidation catalyst. An inverse-structure perovskite photocathode reduces CO_2 and protons to CO and H_2 via a CoMTPP molecular catalyst immobilised on carbon nanotube sheet. An embedded copper wire connects the two photoelectrodes in this artificial leaf configuration.

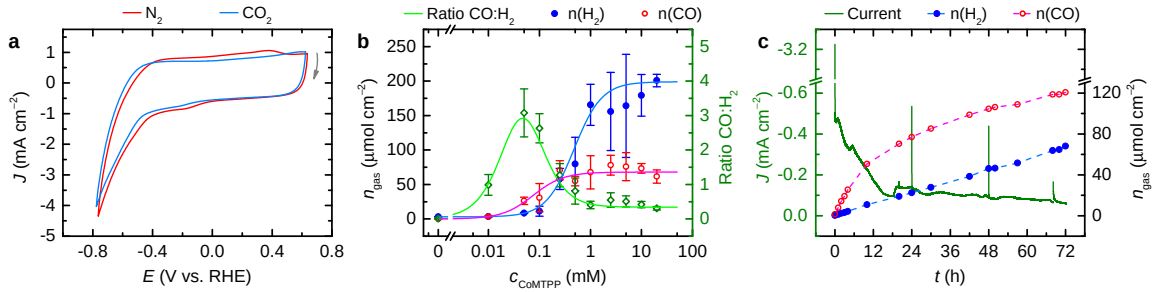

Fig. 2 | Electrocatalysis of CoMTPP@CNT electrodes. a, CV of the buckypaper incubated in the 0.05 mM CoMTPP solution showing an optimal $CO:H_2$ selectivity, recorded under N_2 (pH 9.2) and CO_2 (pH 7.4) atmosphere at a 10 mV s^{-1} scan rate, without stirring. Grey arrow indicates scan start and direction. **b**, Product amounts for electrodes incubated in catalyst solutions of various concentrations and corresponding $CO:H_2$ selectivity after 4 h CPE. A good fit for the $CO:H_2$ ratio (green curve) is found by dividing the sigmoid fits of the gas production. **c**, Long-term CPE test of an electrode incubated in 0.05 mM CoMTPP. Transient capacitive currents are observed at the start of subsequent CPE measurements. **b**,**c**: CPE are recorded at −0.6 V vs. RHE, in a 0.5 M $KHCO_3$ buffer, under CO_2, at room temperature, without stirring.

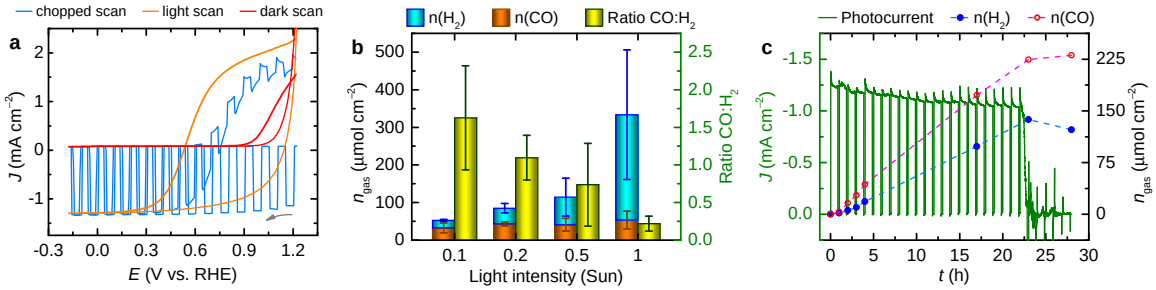

Fig. 3 | PEC performance of the perovskite|CoMTPP@CNT photocathode. a, CV scans of a photocathode under chopped, continuous and no irradiation (0.1 Sun, 0.5 M $KHCO_3$ buffer, 10 mV s^{-1} scan rate, CO_2 atmosphere, pH 7.4, no stirring; grey arrow indicates scan start). CV scans recorded under different light intensities are compared in Supplementary Fig. 16. **b**, Amounts of products and $CO:H_2$ selectivity after 4 h irradiation with different light intensities. **c**, Stability test under 0.1 Sun irradiation and the corresponding product amounts. **b**,**c**: CPE is recorded at 0 V vs. RHE, 0.5 M $KHCO_3$ buffer, under CO_2, room temperature, without stirring, with light chopped in 50 min on, 10 min off intervals.

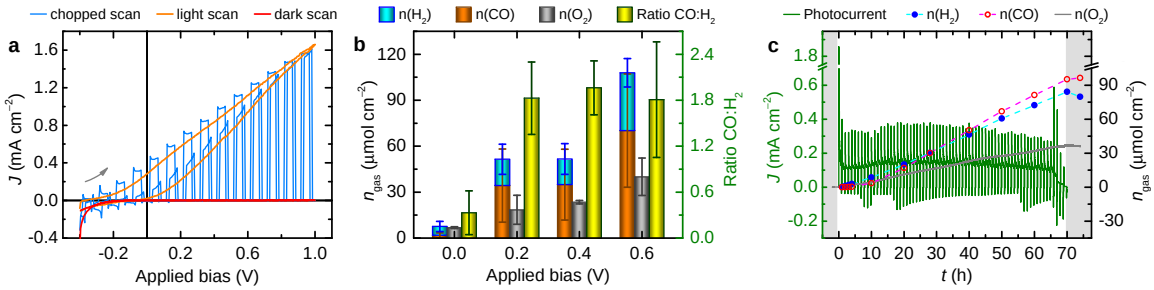

Fig. 4 | PEC of the $BiVO_4$-perovskite|CoMTPP@CNT tandem device. a, CV scans of a PEC tandem under chopped, continuous and no artificial sunlight irradiation (AM1.5G, 100 mW cm^{-2}, 1 Sun, 0.5 M $KHCO_3$ buffer, under CO_2, pH 7.4, room temperature, no stirring; scan start indicated by grey arrow). **b**, Amounts of products and $CO:H_2$ selectivity after 10 h irradiation at different applied bias voltages. **c**, 70 h stability test of a PEC tandem under no applied bias (50 min on, 10 min off light chopping, no stirring). Grey areas indicate open circuit conditions.

obtained by changing the polarity of the rinsing solvent, which potentially affects the catalyst loading near the electrode surface. Accordingly, the highest CO:H_2 ratio of 3.98±0.20 was achieved using chloroform (Supplementary Fig. 7, Table 4). Total faradaic yields (FY) were ≈100% in most cases, with deviations likely due to bubble trapping, solubilised products, capacitive charging of the nanotubes and gas leakage from the PEC cell. The deviations increased at low product amounts of 1-5 μmol cm^{-2}, as gas trapping of even 10 μL, or CNT charging of 0.05-0.1 C can lead to underestimations of up to 50% in the FY. The charging was estimated from the hysteresis in the CV traces and the initial chronoamperometric spikes, which are also visible from Fig. 2a,c (see Supplementary Discussion 1 for a detailed error analysis). IR spectra of ^{13}C labelled products confirmed that CO is solely produced from CO_2 reduction (Supplementary Fig. 8), whereas no formate was detected by ion chromatography, even after a 72 h CPE stability test (Fig. 2c).

Scanning electron microscopy (SEM) and energy-dispersive X-ray (EDX) elemental mapping indicated a homogeneous distribution of the catalyst across the CNT network. No cobalt species could be detected by X-ray photoelectron spectroscopy (XPS) near the top outer surface of buckypaper incubated in 0.05 mM CoMTPP, whereas 10-50 μm catalyst crystals formed on the surface when using the saturated 20 mM solution (Supplementary Figs. 9-11). This indicates that the majority of the catalytically active species detected by ICP-OES is located deeper within the CNT sheet, which may explain the improved selectivity at lower loadings via a high local pH build-up observed in nanostructured electrodes.[28–31] According to recent computational studies, the pH can increase by up to 2-3 units during electroreduction,[32] leading to a local pH of 8-10 inside such nanostructured meshes. The improved selectivity occurs as electroreduction depletes the protons within the pores, leading to a more alkaline local environment, while CO_2 can be replenished by the $KHCO_3 \rightleftarrows H_2CO_3 \rightleftarrows CO_2 + H_2O$ equilibrium. This pH build-up may also contribute to the apparent decrease in the reductive current under CO_2 at a given potential against RHE (Fig. 2a), as the local pH within the CNT matrix varies independently from the bulk solutions' pH.

Perovskite|CoMTPP@CNT photocathodes

An integrated system possessing photocathode functionality was next assembled by interfacing CoMTPP@CNT sheets incubated in a 0.05 mM CoMTPP solution with inverse structure perovskite photovoltaic (PV) cells,[12] using conductive silver epoxy deposited onto a low melting Field's metal alloy. The conductive epoxy provided an electrochemically inert interface to the buckypaper, producing only a negligible amount of H_2 during 4 h CPE at −0.6 V vs. RHE (see Supplementary Table 2). The performance of the 0.25 cm^2 triple cation mixed-halide perovskite PV devices used in this study was consistent with our previous data,[12] with 74 devices averaging a 0.99±0.06 V open circuit voltage (V_{OC}), −17.8±1.7 mA cm^{-2} short circuit current density (J_{SC}), 72.5±5.9% fill factor (FF) and a 12.8±2.1% photovoltaic cell efficiency (PCE) in backward scan direction under 1 Sun irradiation (histograms are shown in Supplementary Fig. 12).

To assess the influence of light intensity on the selectivity towards CO_2 reduction, the photocathodes were characterized under 1, 0.5, 0.2 and 0.1 Sun irradiation (see Fig. 3, Supplementary Fig. 13-18 and Tables 5, 6 for PV and PEC devices). The photocurrent density increased linearly with the light intensity at 0 V vs. RHE (Supplementary Fig. 15), amounting to −5.61±2.90 mA cm^{-2} under 1 Sun irradiation and −1.12±0.10 mA cm^{-2} at 0.1 Sun under continuous operation. 16 out of 24 (67%) perovskite photocathodes employed for the triplicate CPE measurements at different light intensities were stable for at least 4 h indicating a good device reliability (see examples in Supplementary Fig. 17), whereas a long-term test demonstrated stability of up to 23 h at 0.1 Sun (Fig. 3c).

Similar to the electrolysis results at different applied potentials, a lower light irradiation (i.e. a lower photocurrent) correlated with a higher selectivity, with the highest CO:H_2 ratio of 1.63±0.69 obtained at 0.1 Sun, as opposed to only 0.22±0.10 at 1 Sun (Fig. 3b). Stirring improved again the CO:H_2 ratio to 3.66±1.66 at 0.1 Sun (Supplementary Fig. 19). Even though the light intensity limited the absolute current density and the corresponding total amount of products, the FY of CO still increased, indicating that internal transport limitations of proton diffusion from the electrode surface to the inner buckypaper pores also play a beneficial role besides CO_2 transport.[32] The amount of CO generated within 4 h was ≈40 μmol cm^{-2} for all samples.

These results suggest that the devices can offer a steady CO production rate throughout the day even at low light conditions, i.e. from dawn till dusk. This allows maximizing daylight harvesting, as even at moderate 40° latitudes the effective irradiation is below 0.2 Sun for up to 4 h every day, amounting to 0.1-0.7 Sun on cloudy days, and peaking at only ≈0.5 Sun during the cold season (Supplementary Table 7).[33,34] A steady CO production becomes relevant in an industrial context, as CO_2 reduction is the more challenging reaction, whereas H_2 from other sustainable sources may be used to adjust the CO:H_2 ratio in the final collected gas mixture.

$BiVO_4$-perovskite|CoMTPP@CNT tandem devices

The coupling of PEC syngas production to water oxidation was investigated by combining a perovskite|CoMTPP@CNT photocathode and a $BiVO_4$ photoanode with a previously reported Co water oxidation catalyst (WOC) into a back-to-back tandem device[12] (Fig. 1, left side). CV scans of the individual electrodes revealed an overlap at 0.48 V vs. RHE, with a 185 μA cm^{-2} unassisted photocurrent (Supplementary Fig. 20). As the perovskite PV devices provide a V_{OC} of 0.99 V, the PEC tandem would apply an effective potential around −0.5 V vs. RHE onto the CoMTPP@CNT assembly, which is close to the −0.6 V vs. RHE required for optimum CO:H_2 selectivity. The photocurrent of the $BiVO_4$-covered photocathode plateaued at −2.5 mA cm^{-2} around 0 V vs. RHE, corresponding to an effective perovskite irradiation of ≈0.5 Sun, which indicates again that low irradiation must be taken into account even under standard daylight conditions.

The two-electrode tandem system was characterised at different applied biases under 1 Sun irradiation in a one-compartment PEC cell (Fig. 4, Supplementary Figs. 21-28, Table 8, Movie 1). CV scans of the PEC tandems indicated a slightly negative onset potential of approximately −0.2 V for CO_2 reduction (Fig. 4a). A good overlap was observed between the CV traces of the tandem and $BiVO_4$ (Supplementary Fig. 20), proving that the photoanode is the performance-limiting component. 10 h CPE tests confirmed that the tandem configuration provides enough driving force for simultaneous syngas and O_2 generation. The CO:H_2 ratio amounted to 0.33±0.29 under no applied bias with a steady-state photocurrent of 181±20 μA cm^{-2} (Supplementary Fig. 24), whereas a maximum selectivity of 1.96±0.35 was observed at 0.4 V applied bias (Fig. 4b). A similar CO:H_2 selectivity (0.27±0.16) and product amounts were obtained for the bias-free PEC tandems with stirring (Supplementary Fig. 19), as transport limitations play a minor role at absolute photocurrents of only ≈40 μA. Hence, the unassisted tandems may also provide a similar product distribution if employed in a flow device. Solar-to-H_2 and solar-to-CO conversion efficiencies of 0.056±0.028% and 0.018±0.015% were obtained under no applied bias, in-

creasing up to 0.212±0.055% and 0.379±0.174% at 0.6 V bias. Similarly, the production rates of H_2 and CO increased from 0.58±0.33 and 0.18±0.16 μmol cm^{-2} h^{-1} under bias-free operation, to 3.78±0.93 and 7.01±3.70 μmol cm^{-2} h^{-1} at 0.6 V bias. 25 out of 39 (64%) investigated tandems were stable for at least 10 h (see example in Supplementary Fig. 25).

Our PEC tandems presented moderate stabilities within 10 h even under extreme pH conditions, which are typically employed for two-compartment water-splitting electrolysers to avoid pH build-up,[35] but are deemed unsuitable for molecular PEC devices (Supplementary Fig. 22, 23 and Table 8). A strong selectivity towards H_2 formation was observed at pH 1.2 in a 0.5 M $KHCO_3$, 0.5 M H_2SO_4 electrolyte, due to the high proton concentration and loss of the carbonic acid as gaseous CO_2. Alternatively, a low overall CO and H_2 production was observed at pH 13.3 in 0.5 M K_2CO_3, 0.5 M KOH, as the proton concentration is low, while dissolved CO_2 is captured in form of carbonate. These results are in line with existing literature, which shows that optimal CO_2 reduction is conducted at neutral pH values even in high-throughput electrolysers,[36] using buffers acting as a rich CO_2 source where various carbonate species can coexist in a fine equilibrium. More generally, such PEC devices may not require highly corrosive electrolytes, as long as appropriate cell designs are provided.[37,38]

A long-term stability test revealed that a perovskite-$BiVO_4$ tandem could operate at photocurrents higher than 100 μA cm^{-2} for 67 h under no applied bias (Fig. 4c). The tandem produced 96.4 μmol cm^{-2} CO (63.6% FY), 79.8 μmol cm^{-2} H_2 (52.6% FY), and 40.9 μmol cm^{-2} O_2 (57.3% FY). A ≈20% overestimation of the cathodic FY is due to loss of the internal methane standard over the course of three days, while leakage and reduction on the cathodic side lead to a lower O_2 FY. No long-term degradation of the photobsorbers was observed under neutral pH during device operation, as described in Supplementary Discussion 1. This excellent unassisted performance and stability of the PEC tandems was further demonstrated in an artificial leaf configuration (Fig. 1 and Supplementary Fig. 27), with a standalone device producing 25.0 μmol cm^{-2} CO, 45.6 μmol cm^{-2} H_2, and 16.6 μmol cm^{-2} O_2 over the course of 80 h (Supplementary Fig. 26). This greatly improved stability of our devices over other state-of-the-art prototypes,[12,39,40] combined with the material cost[41] and performance[42] advantages of the tandem architecture, indicate that solution immersed perovskite devices are quickly becoming a strong alternative to the more established silicon PV-electrolyzers for the broader PEC field.

Promisingly, the efficiency of the unassisted devices may be enhanced even further by employing inverse-structure perovskite cells with a higher V_{OC},[43] state-of-the-art $BiVO_4$ photoanodes with earlier onset potential and higher photocurrents,[44] or molecular catalysts with lower overpotential requirement for CO_2 reduction,[45,46] which would improve the overlap between the reductive and oxidative photocurrents of the tandem components (Supplementary Fig. 20). A similar effect may be obtained by adjusting the catalyst loading, by varying the relative active areas of the light absorbers and catalysts, or by operating the tandems under concentrated light, as the V_{OC} of solar devices is known to improve at increased light irradiation (Supplementary Fig. 13). In this way, the selectivity could become tunable towards a desirable 0.5 CO:H_2 ratio even without applying external bias. While these strategies may enhance the solar-to-fuel efficiency of perovskite-$BiVO_4$ devices to a certain extent, our approach of interfacing earth abundant molecular catalysts with inorganic light absorbers can also be extended to other state of the art multijunction light absorbers, such as GaAs/InGaP[47] or Si.[48] By targeting CO_2 reduction products requiring low overpotentials (e.g. formate[47], methanol, methane[49] and C_{2+} products) with appropriate catalysts,[21,22,49] higher efficiencies could be also envisioned for such molecular-inorganic hybrid systems.

Conclusions

This work demonstrates a tandem photoelectrochemical device which can sustain unassisted CO_2 to CO conversion coupled to water oxidation. We employ a versatile, precious metal free molecular catalyst which enables us to develop a holistic approach towards tunable syngas production. Accordingly, we look beyond the established strategies of adjusting the CO:H_2 selectivity through the catalyst loading and applied potential, by taking empirical data fitting, solvent fine-tuning and light intensity into account. Resulting perovskite-driven photocathodes present the highest CO selectivity at light intensities as low as 0.1 Sun. This aspect of light management becomes crucial for the carbon economy of industrialized countries, as it maximizes daylight harvesting from dawn till dusk, which may enable the photoelectrochemical conversion of atmospheric CO_2 into CO as a primary source for solar hydrocarbons.

References

[1] Behrens, M. *et al.* The active site of methanol synthesis over Cu/ZnO/Al_2O_3 industrial catalysts. *Science* **336**, 893–897 (2012).

[2] Khodakov, A. Y., Chu, W. & Fongarland, P. Advances in the development of novel cobalt Fischer−Tropsch catalysts for synthesis of long-chain hydrocarbons and clean fuels. *Chem. Rev.* **107**, 1692–1744 (2007).

[3] Bharadwaj, S. S. & Schmidt, L. D. Catalytic partial oxidation of natural gas to syngas. *Fuel Process. Technol.* **42**, 109–127 (1995).

[4] Abdoulmoumine, N., Adhikari, S., Kulkarni, A. & Chattanathan, S. A review on biomass gasification syngas cleanup. *Appl. Energy* **155**, 294–307 (2015).

[5] Graves, C., Ebbesen, S. D., Mogensen, M. & Lackner, K. S. Sustainable hydrocarbon fuels by recycling CO_2 and H_2O with renewable or nuclear energy. *Renewable Sustainable Energy Rev.* **15**, 1–23 (2011).

[6] Shaner, M. R. *et al.* Photoelectrochemistry of core-shell tandem junction n-p^+-Si/n-WO_3 microwire array photoelectrodes. *Energy Environ. Sci.* **7**, 779–790 (2014).

[7] Brillet, J. *et al.* Highly efficient water splitting by a dual-absorber tandem cell. *Nat. Photonics* **6**, 824 (2012).

[8] Pan, L. *et al.* Boosting the performance of Cu_2O photocathodes for unassisted solar water splitting devices. *Nat. Catal.* **1**, 412–420 (2018).

[9] Wang, Q. *et al.* Scalable water splitting on particulate photocatalyst sheets with a solar-to-hydrogen energy conversion efficiency exceeding 1%. *Nat. Mater.* **15**, 611 (2016).

[10] Lu, H. *et al.* Single-source bismuth (transition metal) polyoxovanadate precursors for the scalable synthesis of doped $BiVO_4$ photoanodes. *Adv. Mater.* **30**, 1804033 (2018).

[11] Luo, J. *et al.* Water photolysis at 12.3% efficiency via perovskite photovoltaics and earth-abundant catalysts. *Science* **345**, 1593–1596 (2014).

[12] Andrei, V. *et al.* Scalable triple cation mixed halide perovskite–$BiVO_4$ tandems for bias-free water splitting. *Adv. Energy Mater.* **8**, 1801403 (2018).

[13] Schreier, M. *et al.* Efficient photosynthesis of carbon monoxide from CO_2 using perovskite photovoltaics. *Nat. Commun.* **6**, 7326 (2015).

[14] Jang, Y. J. *et al.* Unbiased sunlight-driven artificial photosynthesis of carbon monoxide from CO_2 using a ZnTe-based photocathode and a perovskite solar cell in tandem. *ACS Nano* **10**, 6980–6987 (2016).

[15] Sokol, K. P. *et al.* Photoreduction of CO_2 with a formate dehydrogenase driven by photosystem II using a semi-artificial Z-scheme architecture. *J. Am. Chem. Soc.* **140**, 16418–16422 (2018).

[16] Li, C. *et al.* Photoelectrochemical CO_2 reduction to adjustable syngas on grain-boundary-mediated a-Si/TiO_2/Au photocathodes with low onset potentials. *Energy Environ. Sci.* **12**, 923–928 (2019).

[17] Sahara, G. *et al.* Photoelectrochemical reduction of CO_2 coupled to water oxidation using a photocathode with a Ru(II)–Re(I) complex photocatalyst and a CoO_x/TaON photoanode. *J. Am. Chem. Soc.* **138**, 14152–14158 (2016).

[18] Urbain, F. *et al.* A prototype reactor for highly selective solar-driven CO_2 reduction to synthesis gas using nanosized earth-abundant catalysts and silicon photovoltaics. *Energy Environ. Sci.* **10**, 2256–2266 (2017).

[19] Arai, T., Sato, S., Sekizawa, K., Suzuki, T. M. & Morikawa, T. Solar-driven CO_2 to CO reduction utilizing H_2O as an electron donor by earth-abundant Mn–bipyridine complex and Ni-modified Fe-oxyhydroxide catalysts activated in a single-compartment reactor. *Chem. Commun.* **55**, 237–240 (2019).

[20] Voiry, D., Shin, H. S., Loh, K. P. & Chhowalla, M. Low-dimensional catalysts for hydrogen evolution and CO_2 reduction. *Nat. Rev. Chem.* **2**, 0105 (2018).

[21] Francke, R., Schille, B. & Roemelt, M. Homogeneously catalyzed electroreduction of carbon dioxide—methods, mechanisms, and catalysts. *Chem. Rev.* **118**, 4631–4701 (2018).

[22] Dalle, K. E. *et al.* Electro- and solar-driven fuel synthesis with first row transition metal complexes. *Chem. Rev.* **119**, 2752–2875 (2019).

[23] Costentin, C., Drouet, S., Robert, M. & Savéant, J.-M. A local proton source enhances CO_2 electroreduction to CO by a molecular Fe catalyst. *Science* **338**, 90–94 (2012).

[24] Lin, S. *et al.* Covalent organic frameworks comprising cobalt porphyrins for catalytic CO_2 reduction in water. *Science* **349**, 1208–1213 (2015).

[25] Zhu, M., Ye, R., Jin, K., Lazouski, N. & Manthiram, K. Elucidating the reactivity and mechanism of CO_2 electroreduction at highly dispersed cobalt phthalocyanine. *ACS Energy Lett.* **3**, 1381–1386 (2018).

[26] Hu, X.-M., Rønne, M. H., Pedersen, S. U., Skrydstrup, T. & Daasbjerg, K. Enhanced catalytic activity of cobalt porphyrin in CO_2 electroreduction upon immobilization on carbon materials. *Angew. Chem. Int. Ed.* **56**, 6468–6472 (2017).

[27] Zhang, X. *et al.* Highly selective and active CO_2 reduction electrocatalysts based on cobalt phthalocyanine/carbon nanotube hybrid structures. *Nat. Commun.* **8**, 14675 (2017).

[28] Li, C. W., Ciston, J. & Kanan, M. W. Electroreduction of carbon monoxide to liquid fuel on oxide-derived nanocrystalline copper. *Nature* **508**, 504 (2014).

[29] Hall, A. S., Yoon, Y., Wuttig, A. & Surendranath, Y. Mesostructure-induced selectivity in CO_2 reduction catalysis. *J. Am. Chem. Soc.* **137**, 14834–14837 (2015).

[30] Ma, M., Trześniewski, B. J., Xie, J. & Smith, W. A. Selective and efficient reduction of carbon dioxide to carbon monoxide on oxide-derived nanostructured silver electrocatalysts. *Angew. Chem. Int. Ed.* **55**, 9748–9752 (2016).

[31] de Luna, P. *et al.* Catalyst electro-redeposition controls morphology and oxidation state for selective carbon dioxide reduction. *Nat. Catal.* **1**, 103–110 (2018).

[32] Suter, S. & Haussener, S. Optimizing mesostructured silver catalysts for selective carbon dioxide conversion into fuels. *Energy Environ. Sci.* **12**, 1668–1678 (2019).

[33] Sharma, A. & Kakkar, A. Forecasting daily global solar irradiance generation using machine learning. *Renewable Sustainable Energy Rev.* **82**, 2254–2269 (2018).

[34] Stoffel, T. & Andreas, A. NREL Solar Radiation Research Laboratory (SRRL): Baseline Measurement System (BMS); Golden, Colorado (Data) (1981). DOI: 10.7799/1052221.

[35] Hernández-Pagán, E. A. *et al.* Resistance and polarization losses in aqueous buffer–membrane electrolytes for water-splitting photoelectrochemical cells. *Energy Environ. Sci.* **5**, 7582–7589 (2012).

[36] Vermaas, D. A. & Smith, W. A. Synergistic electrochemical CO_2 reduction and water oxidation with a bipolar membrane. *ACS Energy Lett.* **1**, 1143–1148 (2016).

[37] Singh, M. R., Xiang, C. & Lewis, N. S. Evaluation of flow schemes for near-neutral pH electrolytes in solar-fuel generators. *Sustainable Energy Fuels* **1**, 458–466 (2017).

[38] McKone, J. R., Lewis, N. S. & Gray, H. B. Will solar-driven water-splitting devices see the light of day? *Chem. Mater.* **26**, 407–414 (2014).

[39] Lee, Y. W. *et al.* Unbiased biocatalytic solar-to-chemical conversion by FeOOH/$BiVO_4$/perovskite tandem structure. *Nat. Commun.* **9**, 4208 (2018).

[40] Zhang, H. *et al.* A sandwich-like organolead halide perovskite photocathode for efficient and durable photoelectrochemical hydrogen evolution in water. *Adv. Energy Mater.* **8**, 1800795 (2018).

[41] Joya, K. S., Joya, Y. F., Ocakoglu, K. & van de Krol, Roel. Water-splitting catalysis and solar fuel devices: Artificial leaves on the move. *Angew. Chem. Int. Ed.* **52**, 10426–10437 (2013).

[42] Hu, S., Xiang, C., Haussener, S., Berger, A. D. & Lewis, N. S. An analysis of the optimal band gaps of light absorbers in integrated tandem photoelectrochemical water-splitting systems. *Energy Environ. Sci.* **6**, 2984–2993 (2013).

[43] Wang, Q., Dong, Q., Li, T., Gruverman, A. & Huang, J. Thin insulating tunneling contacts for efficient and water-resistant perovskite solar cells. *Adv. Mater.* **28**, 6734–6739 (2016).

[44] Qiu, Y. *et al.* Efficient solar-driven water splitting by nanocone $BiVO_4$-perovskite tandem cells. *Sci. Adv.* **2**, e1501764 (2016).

[45] Azcarate, I., Costentin, C., Robert, M. & Savéant, J.-M. Through-space charge interaction substituent effects in molecular catalysis leading to the design of the most efficient catalyst of CO_2-to-CO electrochemical conversion. *J. Am. Chem. Soc.* **138**, 16639–16644 (2016).

[46] Sato, S., Saita, K., Sekizawa, K., Maeda, S. & Morikawa, T. Low-energy electrocatalytic CO_2 reduction in water over Mn-complex catalyst electrode aided by a nanocarbon support and K^+ cations. *ACS Catal.* **8**, 4452–4458 (2018).

[47] Zhou, X. *et al.* Solar-driven reduction of 1 atm of CO_2 to formate at 10% energy-conversion efficiency by use of a TiO_2-protected III–V tandem photoanode in conjunction with a bipolar membrane and a Pd/C cathode. *ACS Energy Lett.* **1**, 764–770 (2016).

[48] Reece, S. Y. *et al.* Wireless solar water splitting using silicon-based semiconductors and earth-abundant catalysts. *Science* **334**, 645–648 (2011).

[49] Rao, H., Schmidt, L. C., Bonin, J. & Robert, M. Visible-light-driven methane formation from CO_2 with a molecular iron catalyst. *Nature* **548**, 74 (2017).

[50] Reuillard, B., Warnan, J., Leung, J. J., Wakerley, D. W. & Reisner, E. A poly(cobaloxime)/carbon nanotube electrode: Freestanding buckypaper with polymer-enhanced H_2-evolution performance. *Angew. Chem. Int. Ed.* **55**, 3952–3957 (2016).

[51] Hoye, Robert L. Z. *et al.* Strongly enhanced photovoltaic performance and defect physics of air-stable bismuth oxyiodide (BiOI). *Adv. Mater.* **29**, 1702176 (2017).

[52] Harris, D. C. *Quantitative chemical analysis* (W.H. Freeman and Co., New York, NY, 2007), 7th ed.

[53] Andrei, V., Reuillard, B. & Reisner, E. Raw data supporting article: Bias-free syngas production by integrating a molecular cobalt catalyst with perovskite-$BiVO_4$ tandems. University of Cambridge Repository. `https://doi.org/` (2019).

Acknowledgements

This work was supported by the Christian Doppler Research Association (Austrian Federal Ministry for Digital and Economic Affairs and the National Foundation for Research, Technology and Development) and the OMV Group (E.R.). V.A. is grateful for the financial support from the Cambridge Trusts (Vice-Chancellor's Award) and the Winton Programme for the Physics of Sustainability. B.R. is grateful to BBSRC (grant number: BB/ K010220/1). XPS data collection was performed at the EPSRC National Facility for Photoelectron spectroscopy ('HarwellXPS'), operated by Cardiff University and UCL, under contract No. PR16195. We gratefully acknowledge Prof. Dominic S. Wright (University of Cambridge) for providing us the Co WOC precursor. We are very grateful to Dr. Demetra Achilleos (University of Cambridge) for help with XPS sample preparation and data analysis. We thank Katarzyna P. Sokol (University of Cambridge) for helpful advice on the O_2 measurements. We also thank Katarzyna P. Sokol and Andreas Wagner (University of Cambridge) for useful feedback on the manuscript.

Author contributions

V.A., B.R. and E.R. designed the project. V.A. prepared the photoelectrodes, performed the experiments, and drafted the manuscript. V.A., B.R. and E.R. analysed the data. B.R. and E.R. contributed to the discussion and completion of the manuscript. E.R. supervised the work.

Competing interests

The authors declare no competing interests.

Methods

Materials. Fluorine doped tin oxide (FTO) glass (~7 Ω/sq, Sigma-Aldrich), $Ni(NO_3)_2 \cdot 6H_2O$ (≥98.5%, Sigma-Aldrich), ethylene glycol (99.8%, anhydrous, ACROS), ethylenediamine (absolute, ≥99.5%, Fluka), PbI_2 (99.99%, for perovskite precursor, TCI), $PbBr_2$ (for perovskite precursor, TCI), formamidinium iodide (Dyesol), methylammonium bromide (Dyesol), N,N-dimethylformamide (DMF; anhydrous, 99.8%, Sigma-Aldrich, and 99%, Alfa Aesar), dimethyl sulfoxide (DMSO; ACS reagent, ≥99.9%, and 99+%, Alfa Aesar), 1-methyl-2-pyrrolidone (NMP; 99.5%, extra dry over molecular sieves, ACROS), chloroform (99.9%, extra dry over molecular sieves, ACROS, and analytical reagent grade, Fischer Scientific), acetonitrile (HPLC grade, Fischer Scientific), [6,6]-Phenyl C_{61} butyric acid methyl ester ([60]PCBM; 99%, Solenne BV), chlorobenzene (extra dry over molecular sieves ≥99.5%, ACROS) polyethylenimine (PEIE; 80% ethoxylated solution, 35-40 wt.% in H_2O, average Mw 70,000, Sigma-Aldrich), isopropanol (IPA; ≥99.5%, Honeywell), Field's metal (ingot, Bi:In:Sn = 32.5:51:16.5 wt.%, Alfa Aesar), $Bi(NO_3)_3 \cdot 5H_2O$ (98%, Sigma-Aldrich), NaI (laboratory reagent grade, Fischer Scientific), p-benzoquinone (≥98%, Sigma-Aldrich), ethanol (absolute, VWR), vanadyl acetylacetonate (≥97.0%, Fluka), NaOH (analytical reagent grade, Fisher), thin multi-wall carbon nanotubes (95+% C purity, Nanocyl-3100), cobalt(II) meso-tetrakis(4-methoxyphenyl)porphyrin (Alfa Aesar), $KHCO_3$ (BioUltra, ≥99.5% (T), Sigma-Aldrich) and $NaH^{13}CO_3$ (98 atom % ^{13}C, 99% (CP), Sigma-Aldrich) were used as purchased without further purification.

CoMTPP@CNT electrodes. The buckypaper was prepared as previously described.[50] Briefly, 30 mg of MWCNTs were dispersed in 150 mL of DMF by sonicating for 2 h. The dispersion was then filtered by vacuum filtration and rinsed with acetone onto a hydrophilic PTFE membrane filter (Omnipore JHWP04700, 0.45 μm pore size, 47 mm diameter). CoMTPP solutions of different concentrations were prepared by dissolving the commercially available catalyst powder in 1.5 mL DMF, or by dilution of a 1 mM solution. A ≈1.0×0.7 cm^2 CNT sheet was incubated for 15-30 min in 0.5 mL of a CoMTPP solution, followed by subsequent rinsing steps in a non-polar solvent and Milli-Q water. After drying, the buckypaper was interfaced to an insulated wire using RS 186-3600 conductive paint, copper tape and epoxy resin, to give an active electrochemical area of ≈1 cm^2.

Perovskite photocathodes. Inverse-structure, triple cation mixed-halide perovskite cells were prepared according to previous reports.[12] Briefly, a 1.0 M $Ni(NO_3)_2 \cdot 6H_2O$, 1.0 M ethylenediamine solution in ethylene glycol was spin-coated using a Laurell WS-650MZ-23NPP instrument onto 1.3×1.3 cm^2 patterned FTO glass and annealed at 573 K to form a NiO_x hole transport layer (HTL).[51] The hot samples were transferred to a N_2-filled glovebox. A cesium formamidinium methylammonium (CsFAMA) mixed-halide perovskite precursor solution was obtained by adding 48 μL of a 1.5 M CsI stock solution in DMSO to 1000 μL of a 1.0 M $FAMA_{0.22}Pb_{1.1}I_{3.2}Br_{0.66}$ solution in DMF (510 μL), DMSO (340 μL), and NMP (150 μL).[12] The precursor solution was spin-coated onto the NiO_x HTL in two-steps, at 1000 RPM for 10 s and 6000 RPM for 35 s, using chloroform as antisolvent. Samples were tempered at 373 K for 30 min. A 35 mg mL^{-1} PCBM solution in chlorobenzene was spin-coated at 3000 RPM for 45 s to form the electron transport layer (ETL). A PEIE solution (3.87 μL mL^{-1} in IPA) was also deposited at 3000 RPM for 30 s. A 100 nm evaporated silver layer formed the top electrical contact, giving a photoactive area of ≈0.5×0.5 cm^2. Catalyst-loaded CNT sheets were attached to Field's metal (FM) foils via RS PRO silver conductive epoxy. The devices were encapsulated by quickly melting and solidifying FM|Ag epoxy|CoMTPP@CNT onto the silver contact of the PV device using a thermoelectric element, then applying Araldite 5-Minute Rapid epoxy onto the exposed edges.[12]

$BiVO_4$|TiCo photoanodes. $BiVO_4$ photoanodes were prepared as reported previously.[12] Briefly, 20 mL of a 0.02 M $Bi(NO_3)_3 \cdot 5H_2O$, 0.4 M NaI aqueous solution (pH adjusted to 1.20 with 68 wt.% HNO_3) was added to 9 mL of a 0.3 M p-benzoquinone solution in ethanol to obtain the BiOI precursor solution. BiOI was electrodeposited onto patterned FTO glass by applying –0.3 V vs. Ag/AgCl for 5 s, then –0.1 V vs. Ag/AgCl for 180 s. 40 μL cm^{-2} of a 0.4 M $VO(acac)_2$ suspension was drop-casted onto the BiOI. The samples were annealed at 723 K for 60 min (1 K min^{-1} ramp rate). Excess V_2O_5 was dissolved from the $BiVO_4$ photoanode by stirring in a 0.2 M NaOH aqueous solution. The Co water oxidation catalyst layer was obtained by repeatedly spin coating 20 μL cm^{-2} of a 4.8 mg mL^{-1} $[Ti_4O(OEt)_{15}(CoCl)]$ solution in dry toluene at 2000 RPM for 10 s under air.

Photovoltaic characterisation. A Sun 2000 Solar Simulator (Abet Technologies) was calibrated to 100 mW cm^{-2} (1 Sun) using a certified RS-OD4 reference silicon diode (1/1.12 mismatch factor). Reverse and forward *J-V* sweeps of the 0.25 cm^2 perovskite devices were recorded between −0.1 and 1.2 V (100 mV s^{-1} scan rate, 0.02 V step) using a Keithley 2635 source meter, in a sealed sample holder under N_2 atmosphere, without masking, at room temperature. The exact active area of individual devices was determined manually. Neutral density filters with 50% and 20% transmission were combined to obtain the 0.1, 0.2 and 0.5 Sun light intensities.

(Photo)electrochemical characterisation. Newport Oriel 67005 solar light simulators with Air Mass 1.5 Global (AM 1.5G) solar filters were calibrated to 100 mW cm^{-2} (1 Sun) using a certified Newport 1916-R optical power meter. The 0.1, 0.2 and 0.5 Sun light intensities were obtained by adding neutral density filters with 50% and 20% transmission. Cyclic voltammetry and chronoamperometry were conducted on PalmSens Multi EmStat^{3+} and Ivium CompactStat potentiostats, with a 0.5 M $KHCO_3$ buffer, at room temperature, without stirring, in gas-tight electrochemical cells purged for at least 30 min before the experiments with N_2 or CO_2 (2% methane internal standard). The CoMTPP@CNT dark electrodes and perovskite|CoMTPP@CNT photocathodes were characterised in a 3-electrode configuration, with the (photo)cathode as working electrode, a $Ag/AgCl/KCl_{(sat)}$ (Basi MW-2030) reference and a platinum mesh counter electrode. A Selemion (AGC Engineering) ion exchange membrane separated the anodic and cathodic compartments. Cyclic voltammetry was typically conducted between −1.4 and 0 V vs. Ag/AgCl for the buckypaper electrodes, −0.2 and 1.2 V vs. RHE for the photocathodes, and −0.4 and 1.0 V for the PEC tandems, at a scan rate of 10 mV s^{-1}. Potentials were converted using the equation E (V vs. RHE) = E (V vs. Ag/AgCl) + 0.059 V×pH + 0.197 V at 298 K. Repeated CV scans were ocasionally conducted to compensate for initial transient charging effects. The tandem devices were characterized in a two electrode configuration, inside a one compartment PEC cell. The front $BiVO_4$ area of the PEC tandems was masked by opaque tape to prevent irradiation of the perovskite photocathode by unfiltered light. No masking was required for the photocathodes in the 3-electrode configuration. CO and H_2 quantification was done by manual sampling from the headspace of the PEC cells into a Shimadzu GC-2010 Plus gas chromatograph (GC). The O_2 evolution was traced using a NeoFox-GT fluorometer and Fospor-R fluorescence oxygen sensor probe from Ocean Optics inside an anhydrous glovebox. Henry's law was used to estimate the amount of dissolved CO, H_2 and O_2 as previously shown.[12]

Materials characterisation. SEM and EDX were recorded on a TESCAN MIRA3 FEG-SEM instrument with an Oxford Instruments Aztec Energy X-maxN 80 system. XPS analysis was performed at the EPSRC National Facility for Photoelectron spectroscopy ('HarwellXPS') using a K-Alpha+ (Thermo Scientific, East Grinstead, UK) spectrometer utilizing a micro-focused monochromatic Al Kα X-ray source (1486.6 eV, 400 μm spot size, 72 W). Survey spectra were collected at a pass energy of 150 eV, whilst high resolution spectra were collected at a pass energy of 40 eV with 10 sweeps. ICP-OES measurements were recorded by Mr. Alan Dickerson (Microanalysis Service, Department of Chemistry, University of Cambridge) on a Thermo Scientific iCAP 7400 ICP-OES DUO spectrometer. Analyte solutions for ICP-OES were obtained by digesting one CoMTPP@CNT sheet in 1.47 mL of >68% HNO_3 and then diluting it to 50 mL with Milli-Q water. TON and TOF were calculated using the Co loading of samples before CPE, unless otherwise stated. IR spectra were obtained with a Thermo Scientific Nicolet iS50 FT-IR spectrometer. Ion chromatography tests were conducted on a Metrohm 882 compact IC plus instrument.

Statistics. Average values are based on triplicates unless otherwise noted, with the errors corresponding to the standard deviation of data points from individual samples. Propagation of uncertainty was taken into account when determining the TOF error from the initial catalyst loading and gas amount.[52]

Data availability

The raw data that support the findings of this study are available from the University of Cambridge data repository, [DOI to be inserted here].[53]